Published in final edited form as:
Oncogene. 2008 March 6; 27(11): 1536–1544. doi:10.1038/sj.onc.1210786.

U19/Eaf2 knockout causes lung adenocarcinoma, B-cell lymphoma, hepatocellular carcinoma and prostatic intraepithelial neoplasia

W Xiao[1,2], **Q Zhang**[1,8], **G Habermacher**[1], **X Yang**[3,4], **A-y Zhang**[1,5], **X Cai**[1], **J Hahn**[1], **J Liu**[5], **M Pins**[3,4], **L Doglio**[6], **R Dhir**[7], **J Gingrich**[5], and **Z Wang**[1,4,5,6]

[1]Department of Urology, Feinberg School of Medicine, Northwestern University, Chicago, IL, USA

[2]Institute of Hydrobiology, Chinese Academy of Sciences, Wuhan, PR China

[3]Department of Pathology, Feinberg School of Medicine, Northwestern University, Chicago, IL, USA

[4]Robert H Lurie Comprehensive Cancer Center, Feinberg School of Medicine, Northwestern University, Chicago, IL, USA

[5]Department of Urology, University of Pittsburgh Cancer Institute, University of Pittsburgh School of Medicine, Pittsburgh, PA, USA

[6]Center for Genetic Medicine, Feinberg School of Medicine, Northwestern University, Chicago, IL, USA

[7]Department of Pathology, University of Pittsburgh Cancer Institute, University of Pittsburgh School of Medicine, Pittsburgh, PA, USA

Abstract

Upregulated gene 19 (U19)/ELL-associated factor 2 (Eaf2) is a potential human tumor suppressor that exhibits frequent allelic loss and downregulation in high-grade prostate cancer. U19/Eaf2, along with its homolog Eaf1, has been reported to regulate transcriptional elongation via interaction with the eleven-nineteen lysine-rich leukemia (ELL) family of proteins. To further explore the tumor-suppressive effects of U19/Eaf2, we constructed and characterized a murine U19/Eaf2-knockout model. Homozygous or heterozygous deletion of U19/Eaf2 resulted in high rates of lung adenocarcinoma, B-cell lymphoma, hepatocellular carcinoma and prostate intraepithelial neoplasia. Within the mouse prostate, U19/Eaf2 deficiency enhanced cell proliferation and increased epithelial cell size. The knockout mice also exhibited cardiac cell hypertrophy. These data indicate a role for U19/Eaf2 in growth suppression and cell size control as well as argue for U19/Eaf2 as a novel tumor suppressor in multiple mouse tissues. The U19/Eaf2 knockout mouse also provides a unique animal model for three important cancers: lung adenocarcinoma, B-cell lymphoma and hepatocellular carcinoma.

Keywords

U19/Eaf2; lung adenocarcinoma; B-cell lymphoma; hepatocellular carcinoma; prostate cancer; tumor suppressor

Correspondence: Dr Z Wang, Department of Urology, University of Pittsburgh, Shadyside Medical Center, Suite G40, 5200 Centre Avenue, Pittsburgh, PA 15232, USA. wangz2@upmc.edu.
[8]Current address: UCLA Immunogenetics Center, Los Angeles, CA 90095, USA.

Introduction

Human upregulated gene 19 (U19)/ELL-associated factor 2 (Eaf2) is a potential prostate tumor suppressor (Xiao *et al*., 2003) that may also participate in acute myeloid leukemia development (Luo *et al*., 2001). However, a definitive role for U19/Eaf2 in tumor suppression remains unclear. Independent studies initially identified U19/Eaf2 as an androgen upregulated gene (U19) in the rat prostate (Wang *et al*., 1997) and as a binding partner for eleven-nineteen lysine-rich leukemia (ELL), making it the second member of the Eaf family of proteins (Simone *et al*., 2001, 2003). U19/Eaf2 shows significant sequence homology to the original family member, Eaf1. ELL was discovered as a fusion partner of MLL in the t(11; 19) (q23; p13.1) chromosomal translocation associated with acute myeloid leukemia (Thirman *et al*., 1994). ELL binds to RNA polymerase II and acts as a transcription elongation factor whose targeted deletion leads to embryonic lethality in mice (Shilatifard *et al*., 1996, 1997a, b; Mitani *et al*., 2000). Eaf2 also appears to be important during embryogenesis, particularly for eye development (Li *et al*., 2003; Maurus *et al*., 2005). Both Eaf1 and U19/Eaf2 stimulate ELL elongation activity (Kong *et al*., 2005). In addition, ELL and Eaf1 colocalize to nuclear suborganelles called Cajal bodies (Polak *et al*., 2003) thought to be involved in nucleoli formation, RNA processing and transport of small ribonucleoproteins (Gall, 2003; Cioce and Lamond, 2005). Studies by Luo *et al.* (2001) argue that the Eaf proteins are important in MLL–ELL leukemogenesis. Our previous studies showed that U19/Eaf2 inhibits xenograft prostate tumor growth and is downregulated in prostate cancer cell lines (Xiao *et al*., 2003). Moreover, a high frequency of loss of heterozygosity (LOH, 82.6%) and homozygous deletion (8%) was noted in high-grade human prostate cancers (Xiao *et al*., 2003). These findings link U19/Eaf2 with two major human cancers—prostate cancer and acute myeloid leukemia.

To further test the hypothesis that U19/Eaf2 is a mammalian tumor suppressor, we constructed and characterized a murine knockout model. The U19/Eaf2 knockout mice develop B-cell lymphoma, lung adenocarcinoma, hepatocellular carcinoma (HCC) and prostatic intraepithelial neoplasia with high frequency.

Results

Generation of U19/Eaf2 knockout mice

We first evaluated the expression pattern of U19/Eaf2 in mice. Using semiquantitative reverse transcription (RT)–PCR, we detected U19/Eaf2 mRNA in all 12 mouse tissues surveyed (Figure 1a). Next, we disrupted the U19/Eaf2 gene by homologous recombination. The mouse U19/Eaf2 gene contains six exons encompassing approximately 34.5 kb of DNA on mouse chromosome 16 while the alternatively spliced isoform lacks exon 3. To create the knockout, a targeting vector was designed to replace exon 2 with a neomycin gene cassette (Figure 1b), resulting in a reading frameshift and termination codons in all three reading frames for both isoforms and deletion of over 85% of the amino acids in U19/Eaf2. Homologous recombination was confirmed in the embryonic stem (ES) cells by PCR and Southern blot analysis (data not shown), and subsequently in the U19/Eaf2 mutant mice (Figures 1c–e). Sequence analysis of the entire open reading frame (ORF) of U19/Eaf2 demonstrated the deletion of exon 2 in both isoforms in the homologous knockout mice (data not shown), while reverse transcriptase–polymerase chain reaction showed the lack of the wild-type U19/Eaf2 transcript (Figure 1f). Western blotting of mouse embryo fibro-blasts (MEFs) isolated from wild-type and U19/Eaf2 knockout mice corroborated the absence of U19/Eaf2 expression in knockouts (Figure 1g). Using real-time RT–PCR, we found no significant difference in Eaf1, ELL1 and ELL2 expression between wild-type and U19/Eaf2-KO specimens from the spleen, liver, kidney and MEF cells (data not shown).

Intercrosses of U19/Eaf2 heterozygous knockout mice in either an isogenic 129P2/Ola Hsd background or in a 129P2/Ola-C57BL/6J mixed genetic background yielded U19/Eaf2-null offspring at Mendelian ratios at birth (data not shown). Within the first 4 months after birth, homozygous mutants and their wild-type littermates were indistinguishable. Given the androgen-dependent regulation of U19/Eaf2 in the prostate, analyses were performed only in male mice.

Using 60 wild-type and 60 U19/Eaf2-null mice for a survival analysis, we found no difference in the viability between these groups up to 4 months of age. No gross abnormalities were observed in the growth of the U19/Eaf2-null mice up to 24 months (data not shown). However, after 4 months, U19/Eaf2-null mice began to die, with 31.8% (19 of 60) mortality reached by 16 months. These mice did not display any overt abnormalities and autopsies did not reveal any macroscopic tumors. Beyond 16 months, sudden death was rare. In contrast, all of the wild-type (Figure 1h) and heterozygous (data not shown) littermates survived throughout the study.

Cardiac enlargement in U19/Eaf2-null mice

Because of the U19/Eaf2-null mice mortality, we did a thorough histological exam of a cohort of null and wild-type animals. Tissues from 6- to 12-month-old U19/Eaf2-null mice revealed no tumors or gross abnormalities in the kidney, lung and brain. However, enlarged hearts were readily apparent in some of the U19/Eaf2-null mice. Cardiac enlargement may be related to cardiac arrest, a possible cause of death especially since no other vital organs displayed abnormalities. Detailed analysis revealed that cardiac enlargement occurred in 39.1% (18 of 46) of U19/Eaf2-homozygous knockout mice (Figure 2a). Specifically, heart/body weight ratio in the effected mice was at least 20% greater than that of wild-type littermates ($P<0.05$; Figure 2b). Histological analysis of cardiac cell density (number cells per unit area) showed a 20% decrease in cell density within the knockout hearts in comparison to wild-type controls (Figure 2c). These findings argue that hypertrophy (larger individual cells), not hyperplasia (greater number of cells), primarily caused the cardiac enlargement (Figure 2c).

Prostatic epithelial hypertrophy, hyperplasia, and dysplasia in U19/Eaf2-null mice

Given the previously discovered tumor-suppressive activity, frequent downregulation and allelic loss of U19/Eaf2 in high-grade human prostate cancer, we focused our analysis on the prostate. Histological examination of the ventral (VP), dorsal (DP), lateral (LP) and anterior prostates (AP) in U19/Eaf2-null males younger than 3 months of age revealed no obvious abnormalities (Figure 3a; data not shown) ($n = 3$ for each group). However, prostate abnormalities were readily apparent by 6 months of age in 11 out of 13 U19/Eaf2-null mice. No abnormalities were observed in age-matched wild-type mice ($n = 10$). The VP and DP lobes of the U19/Eaf2-null mice had a 20–30% increase in wet weight and a more opaque-whitish appearance relative to wild-type controls (Figures 3b and c). Histological examination showed extensive epithelial hypertrophy and hyperplasia in the VP, LP and AP, but not in DP (Figure 3d), possibly reflecting a different differentiation status between the DP and the other prostate lobes. Some focal areas of hyperplastic epithelium displayed severe dysplasia marked by nuclear atypia, including nuclear enlargement and prominent nucleoli (Figure 3d, red arrows) —the hallmarks of mouse prostatic intraepithelial neoplasia (mPIN) (Shappell *et al*., 2004). However, the mPIN noted within the U19/Eaf2-null mice failed to progress to invasive prostate cancers, even at 24 months of age (data not shown). We observed mPINs in 8 out 15 mice aged 24 months. This suggests that the loss of U19/Eaf2 alone may be insufficient to induce high-grade prostate cancer in the mouse. No detectable abnormalities in the stromal layer were observed in U19/Eaf2-null prostates, consistent with the finding that U19/Eaf2 is expressed in epithelial, but not stromal cells (data not shown). Proliferation analysis using an anti-Ki67 antibody in experimental cohorts of six mice aged 6 months demonstrated a 4.5-fold increase in proliferating epithelial cells in the VP of U19/Eaf2-null mice compared to wild type (Figure

3e). In addition, 5-bromo-2-deoxyuridine (BrdU)-labeling in another experimental cohort of 6-month-old mice demonstrated a 5.7-fold increase in labeled VP cells in U19/Eaf2-null mice versus wild-type (Figure 3f). In contrast, terminal transferase dUTP nickend labeling (TUNEL) analysis showed no difference in apoptosis between the wild-type and U19/Eaf2-null prostates (data not shown). These data indicate a major role for U19/Eaf2 in suppressing prostate epithelial proliferation and neoplasia. We also observed a 33% size increase in prostate epithelial cells from knockouts (Figure 3g), suggesting that U19/Eaf2 may also regulate prostate epithelial cell size, as it does within the heart.

Androgens can significantly affect prostate growth, apoptosis and differentiation. To exclude possible secondary effects due to a change in testosterone levels, we measured serum testosterone in all animals examined. No significant difference in serum testosterone was detected between wild-type and U19/Eaf2-null mice (Figure 3h).

Spontaneous tumorigenesis in U19/Eaf2 homozygous and heterozygous knockout mice

A total of 38 homozygotes, 9 heterozygotes and 19 wild-type mice underwent complete histological analysis at 18–24 months (Figure 4). Macroscopic malignant tumors of various histological origins were readily observed in the U19/Eaf2 heterozygotes and homozygotes. The overall tumor incidence was 81.6% (31 of 38) in the homozygous mice and 44.4 % (4 of 9) in the heterozygous mice (Figure 4e). In contrast, only a single (1 of 19 or 5.3%) age-matched wild-type mouse exhibited a macroscopic malignancy (lymphoma) in this analysis (Figure 4e). Hematoxylin and eosin (H&E)-stained tumor sections showed that 52.6% (20 of 38) of the homozygous mice developed adenocarcinoma of the lung, 44.7% (17 of 38) B-cell lymphoma, 31.6% (12 of 38) HCC and 5.2% (2 of 38) skin tumors. Analysis of heterozygous U19/Eaf2 knockout mice revealed a mitigated, but still elevated frequency of lymphoma (22.2% or 2 of 9) and lung adenocarcinoma (22.2% or 2 of 9), but not of HCC (0 of 9). All of these cancers showed typical malignant phenotypes, such as anaplasia and invasiveness. Lymphomas caused dramatic spleen enlargement and were also detected in the liver, lung, kidney, intestine, abdomen and skin (Figure 4c). Immunohistochemical analysis showed that lymphoma cells were positive for B220, but negative for CD3 antigens, pointing to their B-cell origin (Figure 4d).

Ki-67 staining showed that the proliferation rate was much higher in the tumor regions, particularly in the lymphomas (Figures 4a–c). Similar to the prostate tissue, no obvious difference between tumors and normal regions was detected by *in situ* TUNEL analysis, suggesting that U19/Eaf2 deletion did not affect tumor cell apoptosis (data not shown).

U19/Eaf2 is a classic Knudson tumor suppressor

To test whether the carcinogenesis in U19/Eaf2-heterozygous mice was due to haploinsufficiency or LOH, the gene was examined in lymphoma (one from spleen, one from kidney) and lung adenocarcinoma (two) derived from U19/Eaf2-heterozygous mice. The results, using three different markers (AV048865, AV128382 and RH130971) encompassing the mouse U19/Eaf2 allele, indicate that wild-type U19/Eaf2 allele is completely lost in all the tumors examined ($n = 4$) (Figure 5). This argues for U19/Eaf2 as a classic Knudson tumor suppressor instead of a haploinsufficient tumor suppressor (Haber and Harlow, 1997).

U19/Eaf2 overexpression inhibits cell proliferation in vitro

Since U19/Eaf2 affects cell proliferation *in vivo*, we tested if U19/Eaf2 influences cell proliferation and cell cycle regulation *in vitro* using AT6.1 cells, a rat Dunning prostate tumor cell line. We stably transfected the AT6.1 cells with a tamoxifen-inducible U19/Eaf2 expression system (Xiao *et al*., 2003). As expected, U19/Eaf2 overexpression caused dramatic cell growth inhibition both in monolayer culture and soft agar (Figure 6). However, U19/Eaf2

overexpression had no detectable effect on the distribution of cells at different phases of cell cycle in the AT6.1 model (Figure 6).

Discussion

This study describes the first characterization of a murine knockout model targeting an Eaf protein. U19/Eaf2-null and -heterozygous mice spontaneously developed lung adenocarcinoma, B-cell lymphoma and HCC, demonstrating that U19/Eaf2 fits the definition of a tumor suppressor (Haber and Harlow, 1997). In addition, pathologic analysis of prostate tissue from the knockout mice revealed significant PIN, hyperplasia and increases in glandular epithelial cell size.

U19/Eaf2 deletion caused defects starting at least 4 months after birth, suggesting that U19/Eaf2 is required for the maintenance and homeostasis of various tissues in the adult animals rather than for the control of early development. This differed from the previous study showing that inhibition of U19/Eaf2 suppresses eye development in *Xenopus laevis* (Maurus *et al*., 2005), which may be species related.

Our results show that loss of U19/Eaf2 causes an increase in cellular proliferation, consistent with its putative tumor-suppressive activity. Also, U19/Eaf2 knockout mice displayed enlargement of heart cells and prostate glandular epithelial cells, indicating that U19/Eaf2 also plays a role in cell size control *in vivo*. The mechanisms by which U19/Eaf2 influences proliferation and cell size remain unclear; however, U19/Eaf2 deletion did not affect the cell cycle in the AT6.1 model, indicating that it works through a mechanism independent of the cell cycle machinery.

Our previous studies demonstrated that U19/Eaf2 overexpression inhibited prostate cancer cell growth, both in culture and in a xenograft tumor model, via induction of apoptosis (Xiao *et al*., 2003). However, in U19/Eaf2 knockout mice, we did not detect any alterations in apoptosis in prostate tissues, suggesting that endogenous U19/Eaf2 may not cause apoptotic events in the prostate. Thus, our previous observation may have resulted from high expression of U19/Eaf2 in the transfected cells. Alternatively, prostate cancer cells may be sensitized to apoptosis in the presence of U19/Eaf2.

U19/Eaf2 knockout mice did not develop advanced prostate cancer, but the animals did develop precancerous mPIN lesions. U19/Eaf2 inactivation in the human prostate may lead to a more aggressive cancer phenotype than that in the mouse. In fact, studies have demonstrated that the inactivation of certain tumor suppressors, such as VHL or Rb, results in the formation of distinct tumors in humans and mice (Clarke *et al*., 1992; Jacks *et al*., 1992; Haase *et al*., 2001; Ma *et al*., 2003). Thus, U19/Eaf2 inactivation or downregulation in the human prostate may represent a critical step in cancer progression.

U19/Eaf2 has been implicated in human hematopoietic cancers (Luo *et al*., 2001; Simone *et al*., 2001, 2003). The development of B-cell lymphoma in U19/Eaf2 knockout mice argues that U19/Eaf2 is indeed a tumor suppressor in cells of hematopoietic lineage. Simone *et al*. (2003) reported that U19/Eaf2 binds to ELL, a fusion partner of MLL in acute myeloid leukemia, and that the MLL–ELL fusion disrupts the normal binding of ELL to U19/Eaf2. Therefore, the binding of ELL to U19/Eaf2 may regulate proliferation and/or differentiation of hematopoietic cells and the disruption of this binding by the MLL–ELL fusion may contribute to the development of acute myeloid leukemia.

The U19/Eaf2 knockout mouse will provide a powerful animal model for three major cancers: lung adenocarcinoma, B-cell lymphoma and HCC. Although some of the null mice died suddenly before reaching 16 months of age, more than 60% survived past 16 months with a

majority developing macroscopic tumors by 18–24 months. The carcinogenesis in this model is slow, with macroscopic tumors appearing in animals at older age. This rate of development reflects what occurs in most human cancers. Therefore, the U19/Eaf2 knockout mouse may be a promising model for testing novel therapies for these cancers.

In summary, this study defines U19/Eaf2 as a novel tumor suppressor that regulates cell proliferation and size *in vivo*. U19/Eaf2-homozygous and -heterozygous mice develop spontaneous lung adenocarcinoma, B-cell lymphoma, HCC and mPIN, indicating its key role in multiple distinct tissue types and providing an animal model for three major cancers. Downregulation of U19/Eaf2 in human prostate cancer (Xiao *et al*., 2003) and evolutionary conservation of U19/Eaf2 also support a role for U19/Eaf2 as a tumor suppressor in multiple human tissues.

Materials and methods

Generation of U19/Eaf2-null mice

All animal studies outlined within this work were performed in accordance with the Institutional Animal Use and Care Committees. The U19/Eaf2 genomic clone was isolated from λ phage library constructed from 129Sv/J genomic DNA (Stratagene, La Jolla, CA, USA) using mouse U19/Eaf2 cDNA as a probe. The U19/Eaf2 targeting vector was created by cloning a 3.3 kb genomic fragment between the promoter and exon 2, and a 2.8 kb fragment between exons 2 and 3 into the pPNT vector (Tybulewicz *et al*., 1991), which contains a neomycin resistance cassette. The U19/Eaf2 targeting vector was linearized and electroporated into HM1 ES cells (Selfridge *et al*., 1992). Resultant clones were screened for correct homologous recombination by Southern blot analysis. ES clones with a targeted disruption of the U19/Eaf2 locus were injected into C57BL/6J blastocysts to produce chimeric mice. Chimeric males obtained from one targeted ES clone were bred to C57BL/6J or 129P2/Ola Hsd (Harlan, Indianapolis, IN, USA) mice to obtain germ line transmission. The targeted allele has been maintained on a hybrid C57BL/6J/129 strain background, as well as on an inbred 129P2/Ola background. All experiments described here were performed with male mice with a C57BL/6J/129 mixed background. Genotyping of the U19/Eaf2 mutant mice was performed by Southern blot analysis and PCR. The sequence of the primers used for PCR analysis were F1: 5′-CTGGATCTGG TTCTAACTA CCC-3′ (wild-type and mutated forward), R1: 5′-CAAAGTTGATTTT GCTTCCTCTG-3′ (wild-type reverse), KOR1: 5′-GCCAGAGGCCACTTGTGTAG-3′ (mutated reverse) and F2: 5′-CCTGACCAGTGTGGACCTTG-3′ (wild-type and mutated forward). The (F1:R1) was used to detect the wild-type allele, and (F1:KOR1) or (F2:KOR1) was used to detect the mutant allele.

RNA isolation and quantitative RT–PCR of U19/EAF2 expression

Total RNA was isolated from indicated mouse tissues with RNeasy Mini Kit (Qiagen, Valencia, CA, USA) and used as a template for RT or quantitative real-time RT–PCR with primers specific for the U19/Eaf2 transcript. The ribosomal protein L19 was used as control for RNA loading and RNA integrity. The following primers were used: U19/Eaf2 forward 5′-GCTTCTATTGATACTTCTTGTG-3′, U19/Eaf2 reverse 5′ TGGTCATCATCTTCAGAATC-3′; RPL19 forward 5′-ATGAAAT CGCCAATGCCAACTCCC-3′, RPL19 reverse 5′-AGCATTGGCAGTACCCTTCCTCTT-3′. To analyse the sequence of the entire ORF of U19/Eaf2, total RNA was amplified by RT–PCR using the following primers: forward primer 5′-ATGAGTGGACCAGCGGGACTTG-3′, reverse primer 5′-TCAGTCCTCACTGTCGCTTTC-3′.

Western analysis of U19/Eaf2 expression in U19/Eaf2 wild-type and null MEF cells

Primary MEFs were generated from embryonic 12.5(E12.5)- to 13.5(E13.5)-day embryos from a mixed C57BL/6J/129 background. MEFs were immortalized by SV40T antigen (provided by Katherine Rundell) and maintained in Dulbecco's modified Eagle's medium with 10% fetal bovine serum, 0.1 mM nonessential amino acids (Invitrogen, Carlsbad, CA, USA), 100 μM 2-mercaptoethanol (Sigma, St Louis, MO, USA) and penicillin/streptomycin. Western analysis was done on protein lysates from wild-type and U19/Eaf2-null MEFs. Briefly, cells were lysed and protein separated by sodium dodecyl sulfate–polyacrylamide gel electrophoresis. After transfer, membranes were blotted as previously described using an affinity-purified anti-U19/Eaf2 polyclonal antibody (Zhu and Wang, 1999; Xiao *et al*., 2003).

Histological and pathological analysis

Pathological analysis of virgin male mice from 1 to 24 months of age was performed by board-certified pathologists, Drs Ximing Yang, Michael Pins and Rajiv Dhir. Experimental cohorts were wild-type, heterozygous and homozygous littermates with C57BL/6 and 129 combined genetic backgrounds. Tissues were fixed in 10% phosphate-buffered formalin at 4 °C. Samples were embedded in paraffin, sectioned at 5 μm and stained with H&E.

For immunohistochemical staining, tissue sections were deparaffinized using xylene and rehydrated in graded ethanol (EtOH) series. Antigen retrieval was performed in Antigen Retrieval Buffer (BioGene, Kimbolton, UK) by microwaving for 10 min at the highest power. Slides were then equilibrated in phosphate-buffered saline followed by permeabilization in 0.3% Triton X-100. Monoclonal Rat Anti-Mouse Ki-67 antibody (Dako, Glostrup, Denmark) was used for Ki-67 staining according to manufacturer's instructions. Peroxidase In Situ Apoptosis Kit (Chemicon, Temecula, CA, USA) was used for TUNEL assays. Anti-CD3 (Dako) and anti-B220 (BD Pharmingen, San Jose, CA, USA) were used for T- and B-cell staining, respectively. Sections were washed and incubated with biotinylated secondary antibodies and then washed again and incubated with peroxidase streptavidin. Sections were treated with DAB chromagen (Dako) to visualize bound antibody. Slides were then washed in H_2O, dehydrated and coverslips mounted.

BrdU labeling

BrdU labeling reagent and staining kit was purchased from Zymed (Invitrogen). Mice received an intraperitoneal injection of 0.25 ml BrdU labeling reagent 2 h before killing. After killing the mice, tissues were harvested and fixed in 10% buffered formalin. BrdU staining was performed following the protocol provided by the manufacturer.

Loss of heterozygosity analysis

Two lung adenocarcinoma samples, one lymphoma sample from kidney and one lymphoma sample from spleen were dissected from formalin-fixed tissues of the heterozygous mice described in Figure 4e. In addition, normal tissues from the same organs were dissected for use as controls. The dissected tissues were cut into small pieces and thoroughly immersed in a large volume of TE (pH 8.0). The TE buffer was replaced twice over 48 h. The samples were then digested with proteinase K in 50 °C, followed by phenol/chloroform extraction. DNA was dissolved in TE (pH 8.0) for the gene scanning analysis.

After searching the NCBI database, three microsatellite markers (AW048865, AV128382 and RH130971) were found that encompass the mouse U19/Eaf2 allele. 5′6-FAM labeled primers were synthesized and PCR performed for amplification of the U19/Eaf2 allele. The primers for AW 048865: 5′-tactgtggtcctgaagtcgg-3′ and 5′-cctttgggtccaaggaaata. The primers for AV128382: 5′-ggaagactaggggtatgcca-3′ and 5′-gctcacagacagggcataaa. The primers for

RH130971: 5′-tcacattgagttctgtcccaca-3′ and 5′-ctggcatgcaggaagactaggt-3′. The PCR products were sent to Macrogen (Seoul, Korea) for gene scanning analysis.

Serum testosterone measurement

Mouse blood was obtained by cardiac puncture. After spinning in a clinical centrifuge, the serum was collected and stored at −80 °C. Radio immunoassay kits (Diagnostic Systems Laboratories Inc., Webster, TX, USA) were used to measure serum testosterone following manufacture's instructions.

AT6.1 cell cycle analysis

To test the effect of U19/Eaf2 overexpression on the cell cycle, we used GFP-U19-ER, a tamoxifen-inducible U19/Eaf2 expression system (Xiao *et al*., 2003). AT6.1 cells were transfected with the GFP-U19-ER expression vector or the GFP-ER control vector. After 24 h, cells were selected in 1mg ml^{-1} G418 for 10 days. The positive clones were pooled and plated on T-75 flasks, treated with 300 nm 4-hydroxyl-tomaxifen (OHT, Sigma, Atlanta, GA, USA) or vehicle (100% EtOH) for 24 h. The cells were then fixed in 70% EtOH, treated with 100μg ml^{-1} RNase and then stained with 50 μg ml^{-1} propidium iodide (Molecular probes, Eugene, OR, USA). The cell cycle was analysed by FACS (Becton Dickinson, Franklin Lakes, NJ, USA), using XL EXPO 32 software.

AT6.1 cell proliferation assay

AT6.1 cell was plated in six-well plates at about 3000 cells in each well. To activate the GFP-U19-ER fusion protein, 1 m_M 4-OHT in 100% EtOH was added to the culture media to reach a final concentration of 300 n_M. For the control, the same amount of vehicle (EtOH) was added to each well. The cell number was counted using Coulter counter everyday for 3 days after the plating. The experiment was conducted in triplicate.

AT6.1 soft agar assay

Soft agar assays were carried out as described by Kaighn *et al*. (1979). Six-well plates were used for the assay. Cells were harvested and counted using a hemacytometer. About 3000 cells were poured in each well. 4-OHT dissolved in 100% EtOH was added in the bottom and top agar to a final concentration 300 n_M. For the control, the same amount of EtOH was added to the bottom and top agar. After incubation at 37 °C for 7 days, the number of colonies in each well was counted under a dissection microscopy. The experiments were performed in triplicate and repeated twice. No significant difference was detected in parental cell and mock control, but significant difference was detected between AT6.1 stable-transfected GFP-U19/Eaf2-ER with OHT and without OHT.

Acknowledgments

We thank Moira Hitchens for editing, Katherine Rundell for providing reagents, Minh Nguyen for critical reading, Katherine O'Malley and Fei Sufor technical support and members of the Wang lab for extensive discussion. This work was supported in part by NIH R01 DK51193, NIH R01 CA120386, and NIH P50 CA90386 Prostate Cancer SPORE.

References

Cioce M, Lamond AI. Cajal bodies: a long history of discovery. Annu Rev Cell Dev Biol 2005;21:105–131. [PubMed: 16212489]

Clarke AR, Maandag ER, van Roon M, van der Lugt NM, van der Valk M, Hooper ML, et al. Requirement for a functional Rb-1 gene in murine development. Nature 1992;359:328–330. [PubMed: 1406937]

Gall JG. The centennial of the Cajal body. Nat Rev Mol Cell Biol 2003;4:975–980. [PubMed: 14685175]

Haase VH, Glickman JN, Socolovsky M, Jaenisch R. Vascular tumors in livers with targeted inactivation of the von Hippel–Lindau tumor suppressor. Proc Natl Acad Sci USA 2001;98:1583–1588. [PubMed: 11171994]

Haber D, Harlow E. Tumour-suppressor genes: evolving definitions in the genomic age. Nat Genet 1997;16:320–322. [PubMed: 9241260]

Jacks T, Fazeli A, Schmitt EM, Bronson RT, Goodell MA, Weinberg RA. Effects of an Rb mutation in the mouse. Nature 1992;359:295–300. [PubMed: 1406933]

Kaighn ME, Narayan KS, Ohnuki Y, Lechner JF, Jones LW. Establishment and characterization of a human prostatic carcinoma cell line (PC-3). Invest Urol 1979;17:16–23. [PubMed: 447482]

Kong SE, Banks CA, Shilatifard A, Conaway JW, Conaway RC. ELL-associated factors 1 and 2 are positive regulators of RNA polymerase II elongation factor ELL. Proc Natl Acad Sci USA 2005;102:10094–10098. [PubMed: 16006523]

Li M, Wu X, Zhuang F, Jiang S, Jiang M, Liu Y-H. Expression of murine ELL-associated factor 2 (Eaf2) is developmentall regulated. Dev Dynam 2003;228:273–280.

Luo RT, Lavau C, Du C, Simone F, Polak PE, Kawamata S, et al. The elongation domain of ELL is dispensable but its ELL-associated factor 1 interaction domain is essential for MLL-ELL-induced leukemogenesis. Mol Cell Biol 2001;21:5678–5687. [PubMed: 11463848]

Ma W, Tessarollo L, Hong SB, Baba M, Southon E, Back TC, et al. Hepatic vascular tumors, angiectasis in multiple organs, and impaired spermatogenesis in mice with conditional inactivation of the VHL gene. Cancer Res 2003;63:5320–5328. [PubMed: 14500363]

Maurus D, Héligon C, Bürger-Schwärzler A, Brändli AW, Kühl M. Noncanonical Wnt-4 signaling and EAF2 are required for eye development in *Xenopus laevis*. EMBO J 2005;24:1181–1191. [PubMed: 15775981]

Mitani K, Yamagata T, Iida C, Oda H, Maki K, Ichikawa M, et al. Nonredundant roles of the elongation factor MEN in postimplantation development. Biochem Biophys Res Commun 2000;279:563–567. [PubMed: 11118326]

Polak PE, Simone F, Kaberlein JJ, Luo RT, Thirman MJ. ELL and EAF1 are Cajal body components that are disrupted in MLL–ELL leukemia. Mol Biol Cell 2003;14:1517–1528. [PubMed: 12686606]

Selfridge J, Pow AM, McWhir J, Magin TM, Melton DW. Gene targeting using a mouse HPRT minigene/HPRT-deficient embryonic stem cell system: inactivation of the mouse ERCC-gene. Somat Cell Mol Genet 1992;18:325–336. [PubMed: 1440055]

Shappell SB, Thomas GV, Roberts RL, Herbert R, Ittmann MM, Rubin MA, et al. Prostate pathology of genetically engineered mice: definitions and classification. The consensus report from the Bar Harbor meeting of the Mouse Models of Human Cancer Consortium Prostate Pathology Committee. Cancer Res 2004;64:2270–2305. [PubMed: 15026373]

Shilatifard A, Duan DR, Haque D, Florence C, Schubach WH, Conaway JW, et al. ELL2, a new member of an ELL family of RNA polymerase II elongation factors. Proc Natl Acad Sci USA 1997a;94:3639–3643. [PubMed: 9108030]

Shilatifard A, Haque D, Conaway RC, Conaway JW. Structure and function of RNA polymerase II elongation factor ELL. J Biol Chem 1997b;272:22355–22363. [PubMed: 9268387]

Shilatifard A, Lane WS, Jackson KW, Conaway RC, Conaway JW. An RNA polymerase II elongation factor encoded by the human ELL gene. Science 1996;271:1873–1876. [PubMed: 8596958]

Simone F, Luo RT, Polak PE, Kaberlein JJ, Thirman MJ. ELL-associated factor 2 (EAF2), a functional homolog of EAF1 with alternative ELL binding properties. Blood 2003;101:2355–2362. [PubMed: 12446457]

Simone F, Polak PE, Kaberlein JJ, Luo RT, Levitan DA, Thirman MJ. EAF1, a novel ELL-associated factor that is delocalized by expression of the MLL–ELL fusion protein. Blood 2001;98:201–209. [PubMed: 11418481]

Thirman MJ, Levitan DA, Kobayashi H, Simon MC, Rowley JD. Cloning of ELL, a gene that fuses to MLL in a t(11;19)(q23;p13.1) in acute myeloid leukemia. Proc Natl Acad Sci USA 1994;91:12110–12114. [PubMed: 7991593]

Tybulewicz VL, Crawford CE, Jackson PK, Bronson RT, Mulligan RC. Neonatal lethality and lymphopenia in mice with a homozygous disruption of the c-abl proto-oncogene. Cell 1991;65:1153–1163. [PubMed: 2065352]

Wang Z, Tufts R, Haleem R, Cai X. Genes regulated by androgen in the rat ventral prostate. Proc Natl Acad Sci USA 1997;94:12999–13004. [PubMed: 9371789]

Xiao W, Zhang Q, Jiang F, Pins M, Kozlowski JM, Wang Z. Suppression of prostate tumor growth by U19, a novel testosterone-regulated apoptosis inducer. Cancer Res 2003;63:4698–4704. [PubMed: 12907652]

Zhu N, Wang Z. Calreticulin expression is associated with androgen regulation of the sensitivity to calcium ionophore-induced apoptosis in LNCaP prostate cancer cells. Cancer Res 1999;59:1896–1902. [PubMed: 10213498]

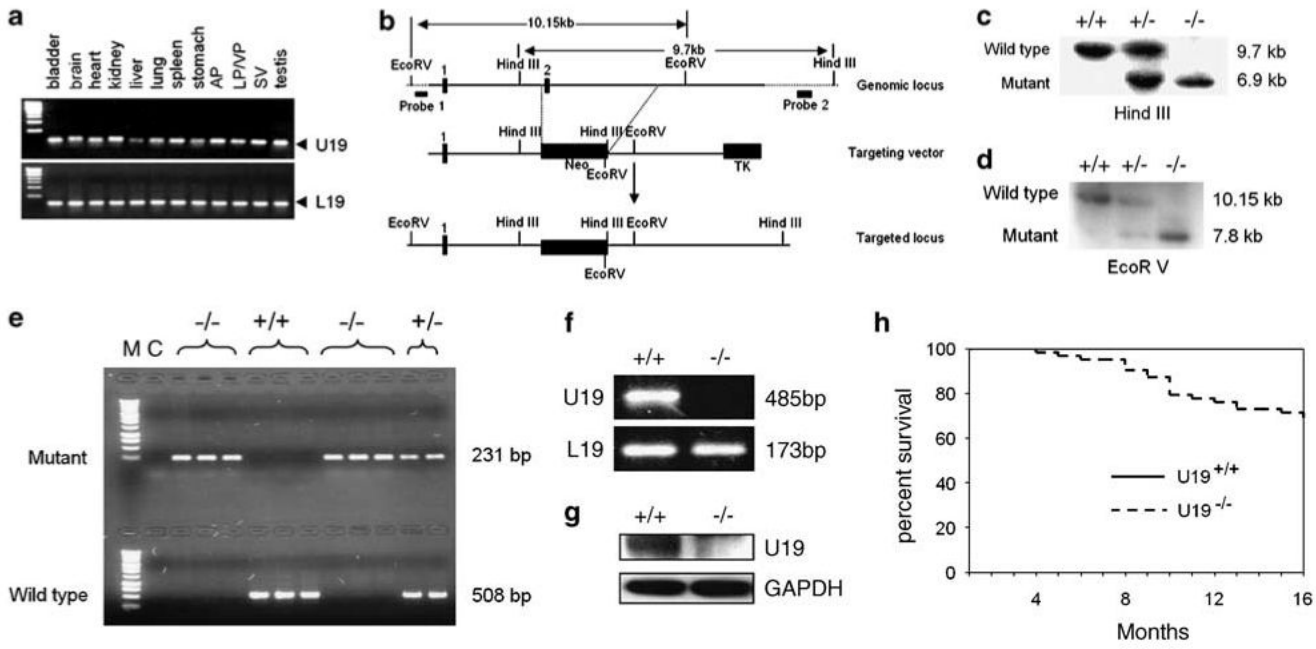

Figure 1.

U19/Eaf2 expression patterns and generation of U19/Eaf2-null mice. (**a**) RT–PCR detection of U19/Eaf2 mRNA and ribosomal protein L19 mRNA (control) in mouse tissues. (**b**) The genomic structure of mouse U19/Eaf2 and the targeting strategy. Exon 2 was replaced with a Neo gene. The positions of probes 1 and 2 for the Southern blot are indicated. (**c** and **d**) Southern blot analysis of genomic DNA, extracted from mouse tail, using the 3′-flanking probe, Probe 2 (**c**), and the 5′-flanking probe, Probe 1 (**d**). (**e**) PCR analysis of mouse tail genomic DNA. PCR primers amplified 508 bp from the wild-type and 231 bp from the targeted allele. M, marker size; C, control without template DNA. (**f**) RT–PCR analysis of U19/Eaf2 mRNA using total RNA from testes of wild-type and knockout mice. The 5′ U19/Eaf2 primer is within exon 2, and the 3′ primer is in exon 5. L19 is the control. (**g**) Endogenous U19/Eaf2 expression in wild-type and U19/Eaf2-null MEFs. Blots of wild-type and U19-null MEFs were probed with antibodies against U19/Eaf2 and glyceraldehyde-3-phosphate dehydrogenase (GAPDH). Experiments were independently done at least twice. (**h**) The survival curve of U19/Eaf2-null mice (n = 60) and their wild-type littermates (n = 60).

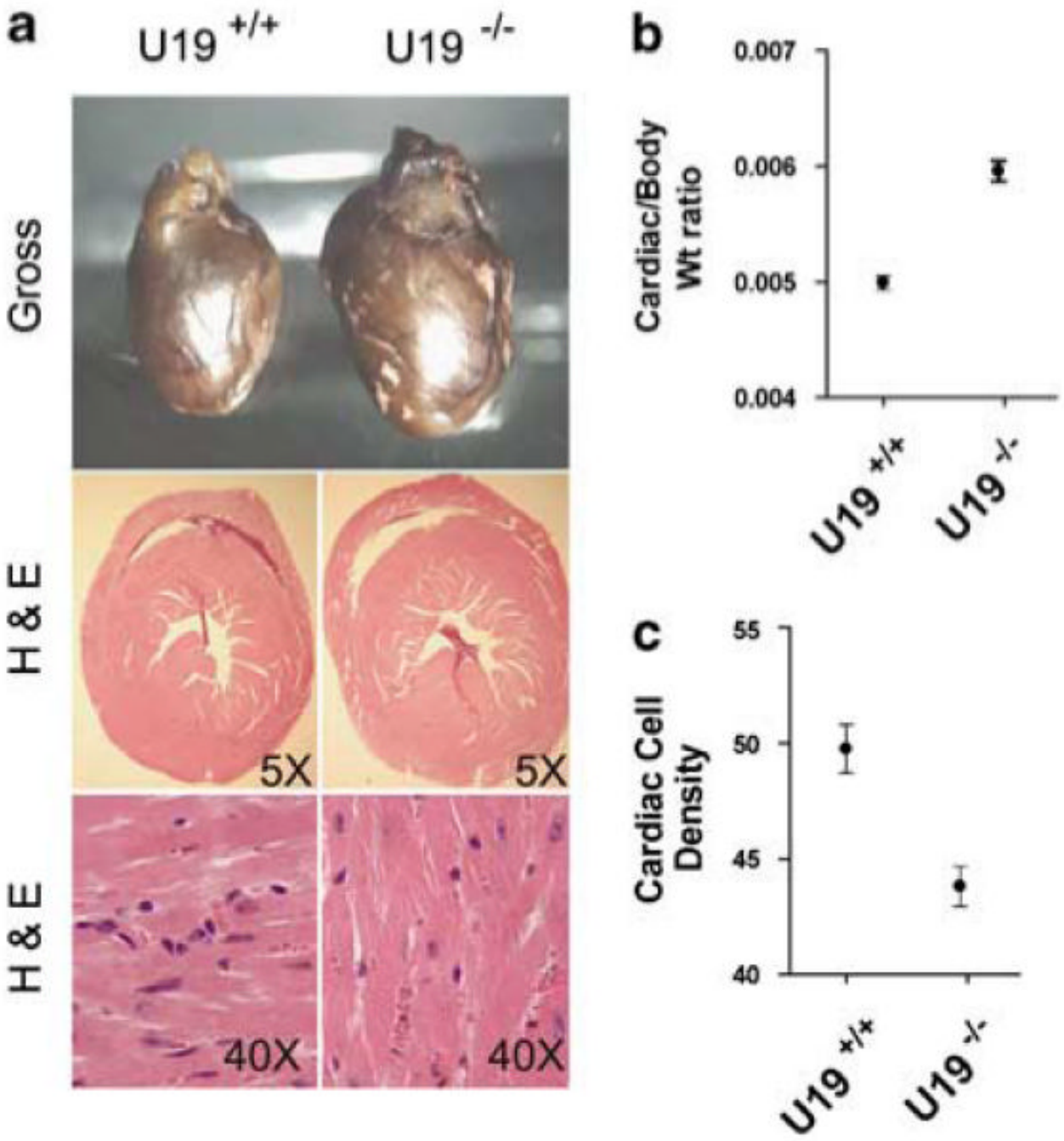

Figure 2.

Cardiac enlargement in U19/Eaf2-null mice. (**a**) Gross morphology and hematoxylin and eosin (H&E) staining (low power and × 40) of a representative wild-type heart and enlarged U19/Eaf2-null heart from 12-month-old mice. (**b**) Heart/body weight ratio. The heart/body weight ratio in effected mice was at least 20% greater than that of wild-type littermates ($P<0.05$). (**c**) Quantitative analysis of cell number in wild-type and enlarged U19/Eaf2-null hearts. The relative cell number per unit area is decreased about 20% in U19/Eaf2-null heart. *$P<0.05$.

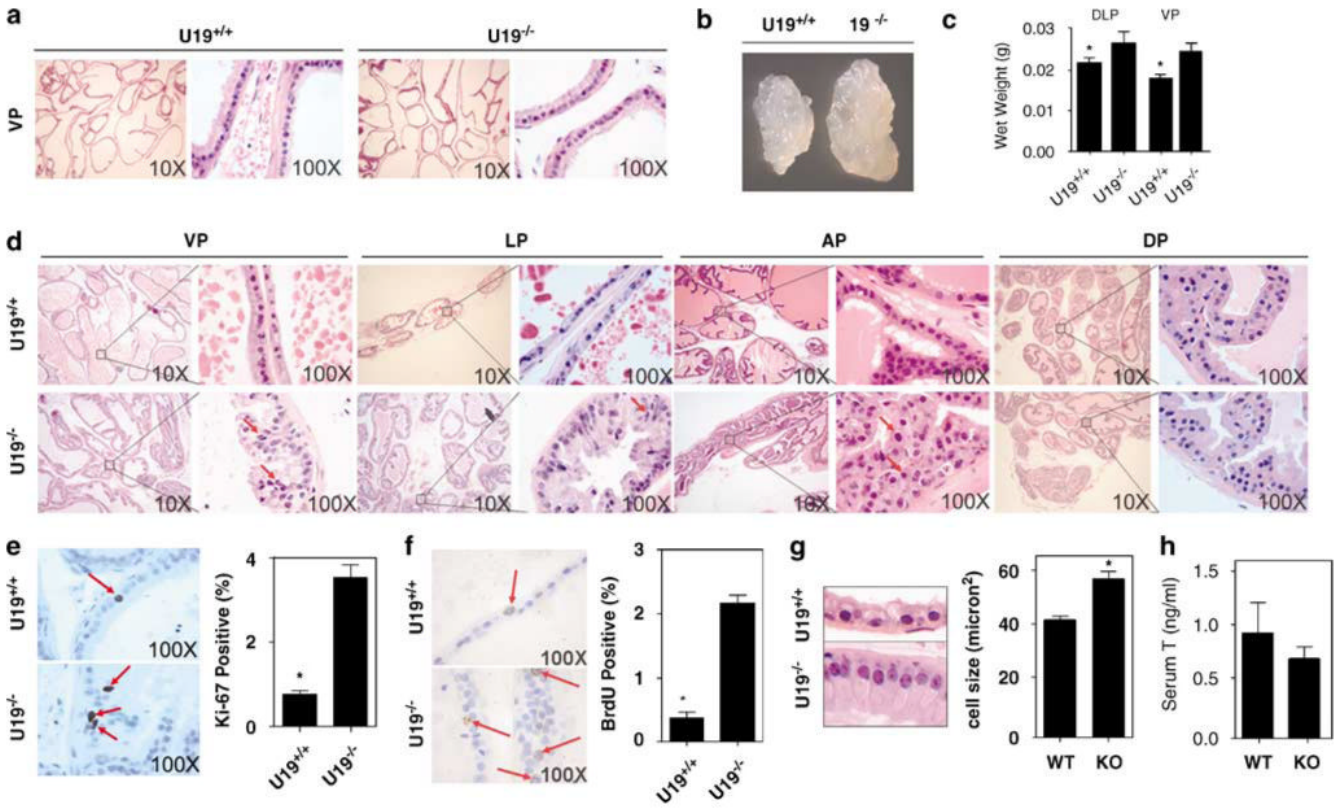

Figure 3.

Prostatic epithelial hypertrophy, hyperplasia and dysplasia in U19/Eaf2-null mice. (**a**) H&E staining of 3-month-old $U19^{+/+}$ and $U19^{-/-}$ ventral prostates (VP). The magnification of the objective is indicated. (**b**) Morphology of 6-month-old $U19^{+/+}$ and $U19^{-/-}$ VPs. U19/Eaf2-null VPs displayed an increase in size and a more opaque-whitish appearance relative to wild-type. (**c**) Wet weight of 6-month-old $U19^{+/+}$ and $U19^{-/-}$ VPs and dorsolateral prostates (DLP). Knockout VPs and DLPs had increased wet weights of approximately 30 and 20%, respectively. **P*<0.05. (**d**) H&E staining of 6-month-old $U19^{+/+}$ and $U19^{-/-}$ ventral (VP), lateral (LP), anterior (AP) and dorsal (DP) prostates. Lower power (× 10 objective) images are shown at left and high power (× 100 objective) images of indicated areas at right. Red arrows mark mPIN. (**e**) Ki67 staining (marked by red arrows) of $U19^{+/+}$ and $U19^{-/-}$ VPs. The stained images (× 100) are shown in the left panel and quantitative analysis in the right panel. **P*< 0.05. (**f**) 5-bromo-2-deoxyuridine (BrdU) labeling (marked by red arrows) of $U19^{+/+}$ and $U19^{-/-}$ VPs. The labeled images are shown in left panel (× 100) and the quantitative analysis in the right panel. **P*<0.05. (**g**) Epithelial cell size of $U19^{+/+}$ (wild type, WT) and $U19^{-/-}$ (knockout, KO) VPs. The H&E staining images, in the left panel, were captured by Leica DFC320 3.3 megapixel color camera at the × 40 objective. The right panel shows the quantitative analysis. The length and width of individual cells were measured to calculate the cell size (length × width). **P*<0.05. (**h**) Serum testosterone (**T**) in wild-type and U19/Eaf2 knockout mice.

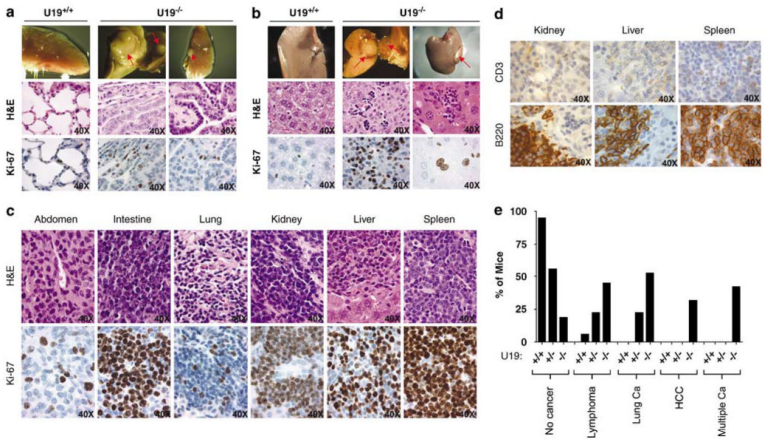

Figure 4.

Macroscopic lung adenocarcinoma, HCC and B-cell lymphoma in U19/Eaf2-null mice, 18–22 months old. (**a**) Morphology, hematoxylin and eosin (H&E) staining (× 40 objective) and Ki-67 staining (× 40 objective) of lungs from one wild-type ($U19^{+/+}$) and two U19-KO ($U19^{-/-}$) mice. One $U19^{-/-}$ mouse developed lung adenocarcinoma (upper images) and the other developed poorly differentiated lung adenocarcinoma (lower images). Ki-67 staining shows more proliferation in tumor regions. (**b**) Morphology, H&E staining (× 40 objectives) and Ki-67 staining (× 40 objective) of livers from one wild type ($U19^{+/+}$) and two U19-KO ($U19^{-/-}$) mice. HCC developed in U19-null mice. Ki-67 staining shows more proliferation in tumor regions. (**c**) H&E staining (× 40 objective), and Ki-67 staining (× 40 objective) of lymphomas in the indicated organs from $U19^{-/-}$ mice. Ki-67 staining shows extremely high proliferation rates in lymphoma sites. (**d**) CD3 and B220 staining of lymphomas in the indicated organs. (**e**) Macroscopic tumor incidence rate in 38 homozygous knockout ($U19^{-/-}$), 9 heterozygous ($U19^{+/-}$) and 19 wild-type ($U19^{+/+}$) mice 18–24 months old. % Mice indicates the % of mice displaying indicated phenotypes. Lung Ca, lung adenocarcinoma; HCC, hepatocellular carcinoma; multiple Ca, different types of cancers observed in the same host.

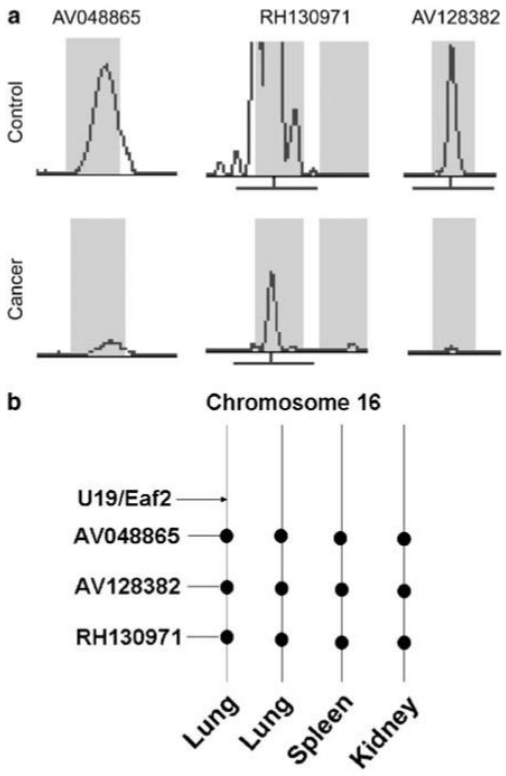

Figure 5.

(**a**) Representative fluorescent electropherograms for microsatellite markers AV048865, RH130971 and AV130971. (**b**) Summary of LOH patterns of four heterozygous tumor samples, two lung adenocarcinoma, one lymphoma from spleen and one lymphoma from kidney. The markers exhibiting allelic loss are indicated in black circles.

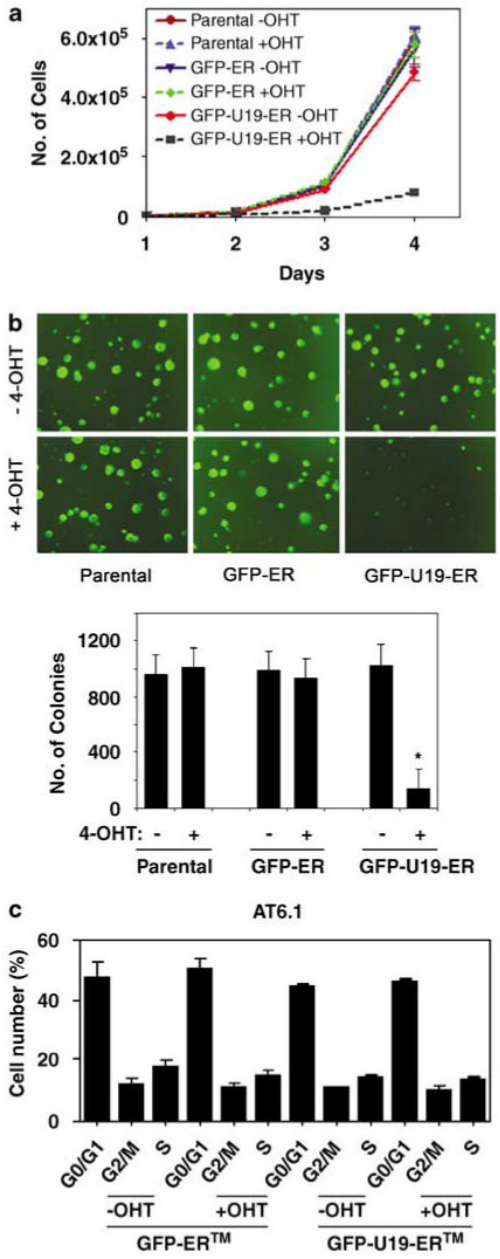

Figure 6.

(**a**) Effect of U19/Eaf2 overexpression on rat Dunning AT6.1 prostate cancer cell proliferation. Parental, green fluorescent protein-estrogen receptor (GFP-ER)-transfected and GFP-U19-ER-transfected AT6.1 cells were plated in six-well plates and the number of cells counted at indicated days in the absence or presence of 300 nM 4-hydroxyl-tomaxifen (4-OHT). The presence of 4-OHT inhibited the proliferation of GFP-U19-ER-transfected AT6.1 cells ($P<0.01$), but not the parental and GFP-ER-transfected AT6.1 cells. (**b**) Effect of U19/Eaf2 overexpression on AT6.1 cell proliferation in soft agar. Parental, GFP-ER-transfected and GFP-U19-ER-transfected AT6.1 cells were plated in six-well plates containing soft agar as described in 'Materials and methods'. Top panel shows representative colonies in the presence or absence of 4-OHT. Bottom panel shows the quantitative analysis of the colony formation. The presence of 4-OHT only inhibited the colony formation of GFP-U19-ER-transfected

AT6.1 cells ($P<0.01$). (**c**) Cell cycle analysis of AT6.1 cells overexpressing U19/Eaf2. No statistically significant difference in the number of G_2/M-phase cells could be detected between AT6.1 cells that overexpress U19/Eaf2 and control AT6.1 cells. Also, 4-OHT did not affect the distribution of the cells at different phases of cell cycle. Results shown as mean of three independent experiments±standard deviation.